Proceedings of the
2016 Annual Conference on Sustainable Research and Innovation,
4 - 6 May 2016

Finite Element Structural Analysis of a Thick-walled Pressure Vessel

Joseph Mutava, Onesmus Muvengei, Kenneth Njoroge and John Kihiu

Abstract—Finite Element Analysis (FEA) is a practical numerical solution tool which can be utilized in determining the stress state in a pressure vessel, especially in local areas such as cavities, O-ring grooves and other areas which would be difficult to analyze manually. A lot of work has been done in developing various numerical and experimental methods to study stresses in pressure vessels. Generally, these studies focus on structural elastic analysis of the pressure vessels since it is a common design practice to aim at maintaining the induced stresses within the elastic region. However, pressure vessels operate under complex environments such as high pressure and temperature, which may lead to gross plastic deformation and subsequent failure. Again, in autofrettage process, the pressure vessel is pressurized beyond the yield point. As a result, the conventional elastic analysis will not be applicable at internal pressures above the yield point. Therefore, it is important to examine the structural integrity of a thick-walled pressure vessel in both elastic and plastic state of the material.

In this study, FE static structural analysis of a presumably uncracked thick-walled pressure vessel has been presented, where stress distribution within the pressure vessel wall and the resulting material deformation were investigated using ANSYS 14.5.7. ANSYS is one of the FE-based design softwares that have become valuable tools in engineering design. Both elastic and plastic analysis were carried out on a plain cylindrical pressure vessel model and on a cylindrical pressure vessel model with a nozzle geometry included. It was observed that the stress distribution in the pressure vessel in the elastic stress state was totally different to that in the plastic stress state. Geometric discontinuity due to a nozzle was found to affect the stress distribution in a large scale. Stress concentration in the areas around the nozzle neck made it impossible to overstrain a thick-walled pressure vessel to a fully plastic state (as required for a fully autofrettaged pressure vessel) without having failed. The FEA results obtained were verified by comparing them with some theoretical results. Better agreement between FEA and theoretical results was obtained for elastic analysis than for plastic analysis. The aim of the study was to contribute to the need of a complete structural analysis of pressure vessels.

Keywords—Finite element analysis, Structural analysis, Thick-walled pressure vessel, ANSYS.

I. INTRODUCTION

PRESSURE vessels have been in wide use for many years in the industrial field. Thick-walled pressure vessels are used for a variety of applications where large pressures are to be withstood. They are usually subjected to high pressures and temperatures which may be constant or cyclic [1]. Such vessels have a multi-axial stress situation where failure is not governed by the individual components of stress but by some combination of all the stress components. Therefore, failure would occur when the stress state somewhere in the wall material exceeds some failure criterion [2]. It is therefore important to be able to understand and quantify or resolve the stresses in a pressure vessel.

The most commonly used factor in the design of pressure vessels is that of maintaining the induced stresses within the elastic region of the construction material in order to avoid excessive plastic deformation or rupture when the yield point is exceeded [3]. Consequently, this has made the study of stresses in pressure vessels to be mainly focused on elastic analysis. Therefore, the conventional elastic analysis of thick-walled pressure vessels would be applicable for internal pressures up to yield point, while in practice, such vessels often undergo pressures above the yield strength of the material [2]. In addition, pressure vessels operate under complex environments such as high pressure and temperature, which may lead to gross plastic deformation and subsequent failure [5]. Moreover, in the process of autofrettage, the pressure vessel is pressurized beyond the yield point so as to cause permanent deformation to some depth from the inner surface, an operation which introduces desirable residual stresses in the wall of the pressure vessel. Therefore, it is important to design and examine the structural integrity of a thick-walled pressure vessel in both elastic and plastic state of the material. This ensures that the full use of the load carrying capacity of the material is accounted for in assessing the structural integrity of the pressure vessel [1].

The design of pressure vessels for operating at very high pressures is a complex problem involving many considerations including definition of the operating and the permissible stress levels, criteria of failure and material behaviour [5]. Therefore, it is difficult to solve such a complex problem by analytical methods. FEA is a practical numerical solution tool which can be utilized in determining the stress state in a pressure vessel, especially in O-ring grooves, and other areas which would be more difficult to analyze manually [7]. FEA provides approximate solutions for complex problems and is widely used for structural analysis [8]. Various commercial softwares like ANSYS, CATIA, ABAQUS AND NASTRAN are available for FEA. In this study, ANSYS was used in carrying out static structural analysis of a presumably uncracked pressure vessel, where stress distribution across the wall thickness and the extent of material deformation that occurs were determined in both elastic and plastic state of the pressure vessel material. Two different geometries of a pressure vessel were considered,

Joseph Mutava, Department of Mechanical Engineering, JKUAT (phone: +254709309 ; e-mail: jsphkioko@yahoo.com).
Onesmus Muvengei, Kenneth Njoroge and John Kihiu, Department of Mechanical Engineering, JKUAT.

one without a nozzle and the other with a nozzle geometry included. Maximum principal (hoop) stress, Von-mises stress and the resulting material deformation were plotted and examined for all cases studied. The results obtained provides some understanding of the effects of plasticity on the stress distribution in a thick-walled pressure vessel, something that cannot be explained by the widely applied conventional elastic analysis by the majority of researchers in this area of study.

II. THEORETICAL BACKGROUND

A. Elastic State of Thick-walled Pressure Vessel

Assuming geometric linearity in material, the state of stress in a thick-walled pressure vessel is tri-axial and it is defined relative to a convenient cylindrical co-ordinate system to give the three principal stresses:

- Hoop (tangential) stress, σ_h
- Radial stress, σ_r
- Longitudinal (axial) stress, σ_l

The following derived equations provide the relationship between the internal pressure (P) and the various principal stresses:

$$\sigma_h = \frac{P{R_1}^2}{{R_2}^2 - {R_1}^2}\left[1 + \frac{{R_2}^2}{r}\right] \tag{1}$$

$$\sigma_r = \frac{P{R_1}^2}{{R_2}^2 - {R_1}^2}\left[1 - \frac{{R_2}^2}{r}\right] \tag{2}$$

$$\sigma_l = \frac{P{R_1}^2}{{R_2}^2 - {R_1}^2} \tag{3}$$

Where:

P - internal pressure
R_1 - inner radius
R_2 - outer radius
r - radial variable

Equation (1) and (2) describe the hoop and radial stress distributions across the wall thickness respectively. Axial stress is independent of r (Eq. (3)) and therefore is constant across the wall thickness. Both hoop and radial stresses are maximum on the inner surface, that is when r is minimum $(r = R_1)$. Radial stress distribution has varying stress from P on the inner surface to zero on the outer. This implies that, the pressure has compressive value of stress equal to internal pressure, P, on the inner surface, which decreases through the wall thickness to zero on the outer surface since gauge pressure there is zero. It is noteworthy that, the stress in the radial direction is always compressive and consequently bears a negative sign. On the other hand, the hoop stress is always a positive value (tensile stress) and among the three principal stresses, it is the maximum and has about twice the the value of longitudinal stress. The hoop and the radial stress distribution across the wall thickness are shown in Figure 1.

Where: $P_i = P$, $r_i = R_1$, $r_o = R_2$, $\sigma_t = \sigma_h$ and σ_o is the outer surface gauge pressure which is equal to zero.

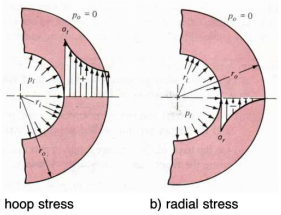

Fig. 1. Hoop and radial stress distribution within the pressure vessel wall

The maximum shear stress (Eq. 11) also occurs on the inner surface of the vessel, just as does both tensile (hoop) and compressive (radial) stresses.

B. Elastic-plastic state of Thick-walled pressure vessel

In thick-walled pressure vessels, stress is directly proportional to strain up to yield point. Beyond the yield point, there comes a phase (elastic-plastic) in which partly the material is elastic and partly plastic [1] as shown in Figure 2.

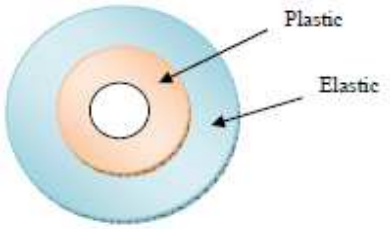

Fig. 2. Elastic-plastic region across the wall thickness

As the internal pressure is increased beyond the yield point, the plastic region also increases proportionally to the pressure until the whole material becomes plastic. The stress state of the plastic region shown as 2 in Figure 3 is represented as power law:

$$\sigma = E_T \epsilon^n \tag{4}$$

Where:

σ - Stress
E_T - strain hardening modulus
n - Strain hardening exponent which ranges from 0 to 1

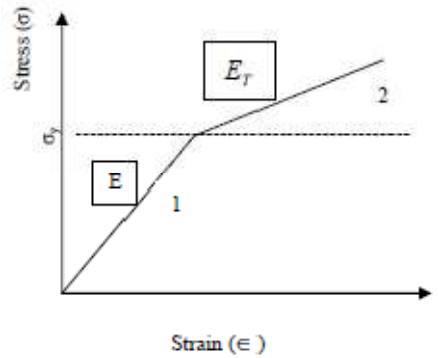

Fig. 3. Stress-strain curve with strain hardening

Where:

1 - Elastic region where E (Young's Modulus) applies
2 - Plastic region where E_T applies
σ_y - Yield strength

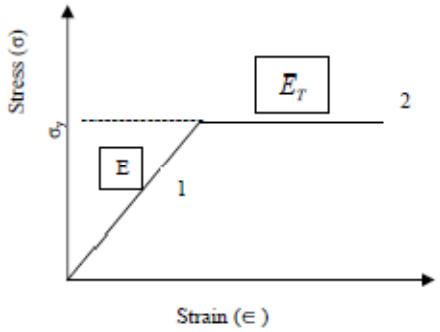

Fig. 4. Stress-strain curve without strain hardening

Plastic materials with strain hardening necessitate increasingly higher stresses to result in further plastic deformation. Since the strain hardening for most high strength engineering materials is considerably less than 0.2, the increased complexity introduced by considering strain hardening is generally not necessary within the partially plastic region [9]. Therefore, the material behaviour model that is generally used for pressure vessel design is the elastic-perfectly plastic representation (Figure 4), which assumes zero strain hardening [9].

From Figure 4, it can be deduced that the material has a lower load carrying capacity than one in which strain hardening is present (Figure 3). In the simplified model, the proportional limits (σ_y) as well as the ultimate strength are identical. A thick-walled pressure vessel would be fully plastic when the stress in the full wall cross-section reaches the yield stress like in the case of fully autofrettaged pressure vessel.

In autofrettage, the material is loaded until it attains elastic-plastic state. Autofrettage is a common process of producing residual stresses in the wall of a thick pressure vessel prior to its use [10]. An appropriate pressure, large enough to cause yielding within the wall, is applied to the inner wall of the vessel and then removed. Large scale yielding occurs in the autofrettaged pressure vessel wall [10]. Upon the release of this pressure, a compressive residual stress is developed to a radial depth at the bore. These residual stresses serve to reduce the tensile stresses developed as a result of subsequent application of an operating pressure thus increasing the load bearing capacity [10]. In addition, autofrettage increases the material's resistance to stress cracking of the pressure vessel and as result enhances the fatigue life of the pressure vessel [11].

The governing equations for formulating stress distribution for the elastic-plastic region have been derived by considering the power law (Eq. (4)) based on modified Von Mises yield criterion for axially symmetric thick-walled pressure vessel [1]. Consider a plain strain thick-walled cylinder subjected to internal pressure (P). When the pressure is large enough, the cylinder begins to yield from the inner surface (at $r = R_1$). There exists a radius, r_c, at the elastic and plastic boundary interface [1]. Therefore, the material can be analyzed as region between plastic region (where: $R_1 < r < r_c$) and elastic region (where: $r_c < r < R_2$) [1].

The following pressure, P, radial stress, σ_r and hoop (circumferential) stress, σ_h equations are obtained [1]:

$$P = \frac{\sigma_y}{\sqrt{3}}\left[1 - \frac{r_c^2}{R_2^2} + 2ln\frac{r_c}{R_1}\right] \tag{5}$$

$$\sigma_r = \frac{\sigma_y}{\sqrt{3}}\left[-1 + \frac{r_c^2}{R_2^2} - 2ln\frac{r_c}{R_1}\right] \tag{6}$$

$$\sigma_h = \frac{\sigma_y}{\sqrt{3}}\left[1 + \frac{r_c^2}{R_2^2} - 2ln\frac{r_c}{R_1}\right] \tag{7}$$

The main assumption in deriving Eqns. (5), (6) and (7) is that external pressure is taken to be zero [1].

The internal pressure required at the onset of yielding (P_{y1}) at the inner wall surface and the internal pressure required in order to cause the full wall cross-section to yield completely (P_{y2}) are given by [10]:

$$P_{y1} = \frac{K^2 - 1}{\sqrt{3}K^2}\sigma_y \tag{8}$$

$$P_{y2} = \frac{K^2 - 1}{\sqrt{3}}\sigma_y \tag{9}$$

Where:

$$K = \frac{R_2}{R_1} \tag{10}$$

The equation that describes the longitudinal (axial) stress induced in the wall of the thick-walled pressure vessel remains unchanged even after loading beyond the yield point and therefore is given by Eq. (3).

C. Failure Theories

In traditional structural design, which uses a strength-of-material approach, the stress analysis alone cannot be able to predict the failure of a structural component [4]. Therefore, various failure theories have been derived to combine and measure the induced stresses against the potential failure mode. The most commonly used theories of failure are [9]:

- Maximum principal stress theory (Rankine's failure theory)
- Maximum shear stress theory (Tresca's failure theory)
- Maximum distortion energy theory (Von Mises failure theory)

According to the maximum principal stress theory, failure occurs when one of the three principal stresses reaches a stress value of elastic limit as determined from a uniaxial tension test. This theory is meaningful for brittle fracture situations [9].

The maximum shear stress theory states that, the maximum shear equals the shear stress at the elastic limit as determined from the uniaxial tension test [9]. For a triaxial stress system, the maximum shear stress is given as:

$$\tau_{max} = \frac{\sigma_1 - \sigma_2}{2} = \frac{\sigma_y}{2} \quad (11)$$

The distortion energy theory considers failure to have occurred when the distortion energy accumulated in the component under stress reaches the elastic limit as determined by the distortion energy in a uniaxial tension test [9]. This failure criterion states that yielding will take place when:

$$(\sigma_1 - \sigma_2)^2 + (\sigma_2 - \sigma_3)^2 + (\sigma_3 - \sigma_1)^2 = 2\sigma_y^2 \quad (12)$$

Where, in all the cases:

σ_1 - first principal stress
σ_2 - second principal stress
σ_3 - third principal stress
σ_y - yield stress

Such that: $\sigma_1 > \sigma_2 > \sigma_3$

Among the failure theories, Von Mises criterion is generally accepted to be better suited for common pressure vessels as it is found to be more accurate [9]. Trescas criterion is commonly used for the design by analysis procedure for two reasons [9]: It is more conservative and it is considered easier to apply. However, with the availability of computers, it has also made it easier to apply the Von Mises criteria.

D. Stress Intensity

The stress intensity, S, is the maximum value of the stress differences, where the stress differences are the algebraic differences of the principal stresses [9]. Therefore:

$$S = (\sigma_1 - \sigma_3) \quad (13)$$

In terms of stress intensity, S, Trescas criterion reduces to:

$$S = \sigma_y \quad (14)$$

III. STRUCTURAL ANALYSIS BY ANSYS

In this study, the investigated thick-walled pressure vessel is presumably made of $34CrMo4$ alloy steel, which has been increasingly applied to the design and manufacture of pressure vessel and piping [5]. The material has Young's Modulus of $206 \times 10^3 3MPa$, Tensile strength of $837MPa$, Yield strength of $743MPa$ and Poissons ratio of 0.3. The alloy steel was assumed to be isotropic linear-elastic when loaded below yield point for FE elastic analysis and to be isotropic elastic-perfectly plastic when loaded beyond its yield strength for FE plastic analysis.

Three-dimensional $(3D)$ solid model was used for all the pressure vessel geometries considered, where the various geometrical size conditions are as indicated in Table I. Length of the model was taken as $150\ mm$ in all cases. Where nozzle geometry was included, a diameter of $20\ mm$ and a length of $30\ mm$ projected above the outer surface were taken. Symmetry boundary conditions were invoked such that only an eighth model of the pressure was used with appropriate boundary conditions applied.

Since hoop stress (first principal stress) is always the maximum among the three resulting principal stresses, its distribution in the pressure vessel wall was examined. Von Mises failure criterion is said to be relatively more accurate in predicting failure in pressure vessels and therefore the resulting Von Mises stress was also investigated in this study.

For thick-walled pressure vessel, the wall thickness is relatively large and the stress variation within the wall needs to be understood. Therefore, the distribution of the hoop and Von misses stresses across the wall thickness were also investigated.

The amount of deformation of the pressure vessel due to internal pressure loading was also examined. The resulting deformation was given in terms of resultant (vector sum) displacement measured in millimetres.

TABLE I
GEOMETRICAL SIZES OF PRESSURE VESSEL

Geometry	Inner radius R_1(mm)	Outer radius R_2(mm)	Wall thickness t(mm)	$\frac{R_1}{t}$
Without a nozzle	45	60	15	3
	75	90	15	5
	120	135	15	8
	150	165	15	10
With a nozzle	45	60	15	3
	75	90	15	5
	120	135	15	8
	150	165	15	10

A. FE Structural Elastic Analysis of a Thick-walled Pressure Vessel Without a Nozzle

The various thick-walled pressure vessel geometrical sizes, as depicted in Table I, were modeled in ANSYS. The first case to be modeled was that of a pressure vessel with inner radius to wall thickness ratio (R_1/t) of 5 (the average size), whose $3D$ section model without a nozzle is as shown in Figure 5. "Path A" indicates the path along which stress distribution across the wall thickness was examined. Boundary conditions were applied on the surfaces clearly marked in Figure 6 by small 's' symbols. This was done by simply defining symmetry boundary conditions on the relevant areas.

The model was meshed using SOLID186, a higher order $3D$ 20-node solid element that exhibits quadratic displacement behaviour. This type of element was chosen as it supports both elasticity and plasticity and therefore it would be suitable for this study. An element edge length of $7.5\ mm$ was chosen, which gave good results. The meshed model is shown in Figure 7.

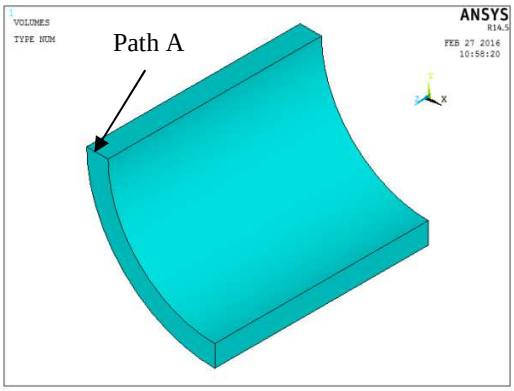

Fig. 5. An eighth section model without nozzle

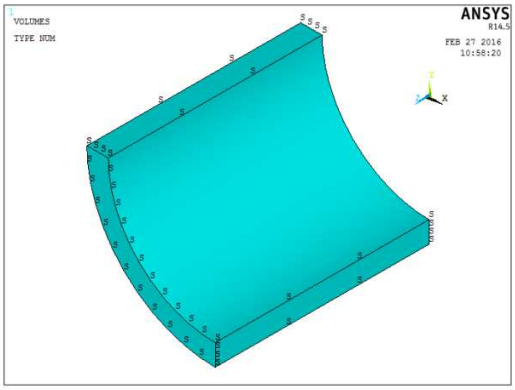

Fig. 6. Boundary condition areas on model without nozzle

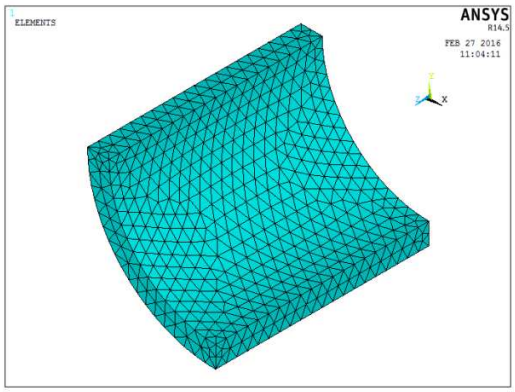

Fig. 7. Meshed model without nozzle

A working pressure load of 38MPa (calculated using Eq. 1) was applied on the inner surface of the model and an end effect pressure force of $86.3636MPa$ (calculated from Eq. (3)) was applied on the rear end surface of the model in order to account for the axial tensile load due to the internal pressure in a closed pressure vessel. The value of the working pressure was obtained from the tensile strength of the material $(837MPa)$ with the application of an appropriate factor of safety of 4. The model was considered ready for solution after creating the mesh, applying the appropriate material properties and boundary conditions and finally after applying the loads to the model.

Similarly, the other geometrical sizes of R_1 to t ratio of 3, 8 and 10 were modeled and analysed the same way as has been outlined for the average size geometry.

B. FE Structural Elastic Analysis of a Thick-walled Pressure Vessel With a Nozzle

The same geometrical sizes (see table 1) dealt with in the elastic analysis of a thick-walled pressure vessel that does not have a nozzle were also considered in a case where nozzle geometry was included. A $3D$ section model of a pressure vessel whose geometrical size is characterized by R_1 to t ratio of 5 is shown in Figure 8. "Path B" shows the path around the nozzle neck along which stress distribution within the wall thickness was examined.

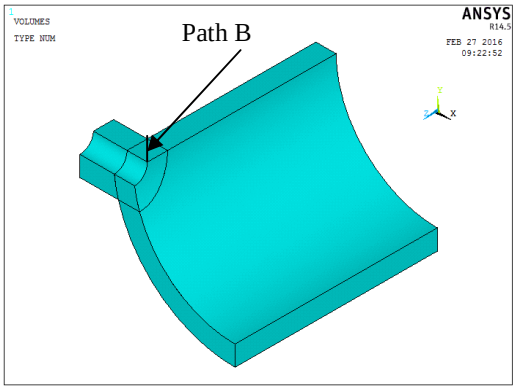

Fig. 8. An eighth section model with nozzle

Figure 9 illustrates the areas where boundary conditions were applied. The same element type and element edge length as used before were maintained for this analysis. The meshed model is as shown in Figure 10.

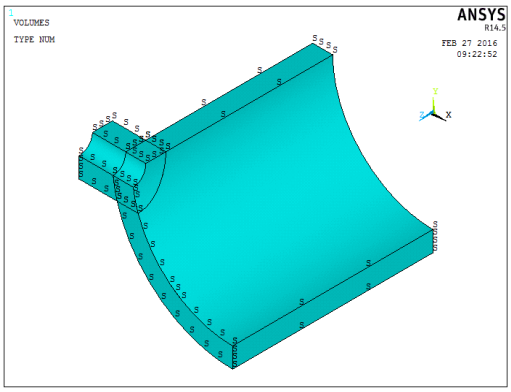

Fig. 9. Boundary condition areas on model with nozzle

The same working pressure and end effect force was also maintained. The working pressure was applied on the inner surface including the nozzle internal surface as well. An end effect force of $7.2381MPa$ (calculated using Eq. (3)) was applied on the cut end surface of the nozzle, in order to account for the pulling effect of the nozzle. Finally, solution of the model was done.

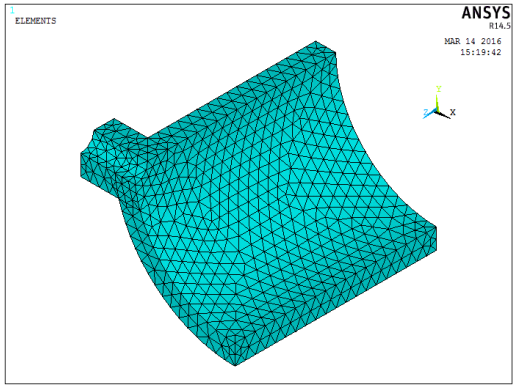

Fig. 10. Meshed model with nozzle

Similarly, the same analysis was carried out for the other three geometrical sizes of thick-walled pressure vessel set for consideration in this study (see table I).

C. FE Structural Plastic Analysis of a Thick-walled Pressure Vessel Without a Nozzle

The same geometrical sizes of thick-walled pressure vessel dealt with under elastic analysis were likewise considered for plastic analysis. A $3D$ section model similar to the one shown in Figure 5 was used. The type of element and element edge length were maintained as in the earlier analyses. Plasticity was appropriately included in the FE modeling and the stress-strain curve which was obtained (Figure 11) depicts the material's structural behaviour model. The curve resembles the theoretical one presented in Figure 4.

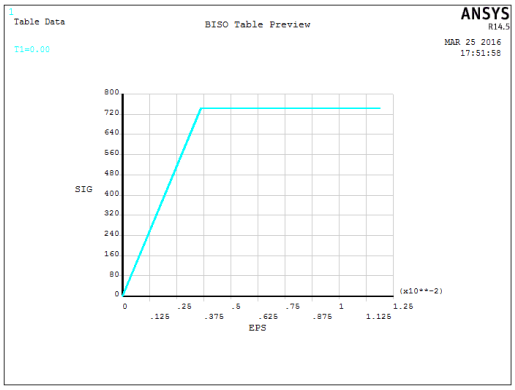

Fig. 11. FE plastic stress-strain curve without strain hardening

Two categories were considered: one with plastic region estimate of $5mm$ depth and another one with estimated plastic region depth of $10mm$.

1) FE Plastic Analysis - Plastic Region of $5mm$ *Depth:* The following parameters were computed and applied for a geometrical size of $R_1/t = 5\ mm$:

- Working pressure of $145MPa$ (calculated from Eq. (5)), which was estimated to cause a plastic region of $5mm$ depth (i.e. $r_c = 80mm$) from the inner surface of the pressure vessel wall.
- End effect pressure force of $330.45MPa$ (calculated from Eq. (3))

The meshed model was similar to the one shown in Figure 7.

A similar analysis was done for all the other three geometrical sizes. In all the cases considered, plastic region depth of $5\ mm$ from the inner surface of the vessel was estimated.

2) FE Plastic Analysis - Plastic Region of $10\ mm$ *Depth:* The following parameters were computed and applied for a geometrical size of $R_1/t = 5\ mm$:

- Working pressure of $153.72MPa$ (calculated from Eq. (5)), which was estimated to cause a plastic region of $10\ mm$ depth (i.e. $r_c = 85\ mm$) from the inner surface of the pressure vessel wall.
- End effect pressure force of $349.36MPa$ (calculated from Eq. (3))

The meshed model was also similar to the one shown in Figure 7.

A similar analysis was done for all the other geometrical sizes, where in all the cases considered, a size of the plastic region of $10\ mm$ depth from the inner surface of the vessel was estimated.

D. FE Structural Plastic Analysis of Thick-walled Pressure Vessel With a Nozzle

A $3D$ section model of the average geometrical size ($R_1/t = 5$) similar to the one shown in Figure 8 was used. Descretization of the model was done as previously discussed with the same type of element chosen and the meshed model was the same as the one illustrated in Figure 10. Plasticity was appropriately included and the resulting stress-strain curve was the same as the one presented in Figure 11. Loading of the model was suitably computed using the relevant equations, where an internal pressure of $145.4MPa$ was applied on the inner surface of the model including that of the nozzle. An end effect pressure force of $330.45MPa$ and $27.7MPa$ was respectively applied on the rear end surface of the model and on the end surface of the nozzle. A plastic region of $5mm$ depth ($r_c = 80mm$) was estimated in the analysis.

Similar analysis was done for all the other geometrical sizes which were set for consideration in this study. An attempt to consider a case (like the previous) with an increased plastic region depth to $10\ mm$ failed to solve the problem, where the outcome report indicated that, the component was improperly constrained.

IV. RESULTS AND DISCUSSION

The FEA results obtained were compared with some calculated results in order to verify them. It is important to compare FEA results with appropriate theoretical results whenever possible so as to validate the results. However, FEA is presumably applied because a theoretical solution is not available, especially for complicated problems. In such cases, experimental results may be sought to validate the FEA results.

A. Elastic Analysis Results - Thick-walled Pressure Vessel Without a Nozzle

Figure 12 and 13 illustrates the FEA results for hoop and Von mises stress in the pressure vessel wall.

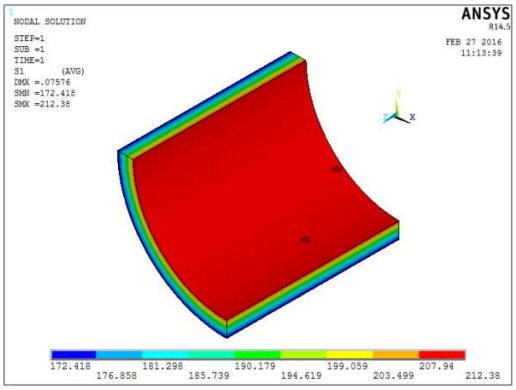

Fig. 12. Hoop stress - Elastic model without nozzle

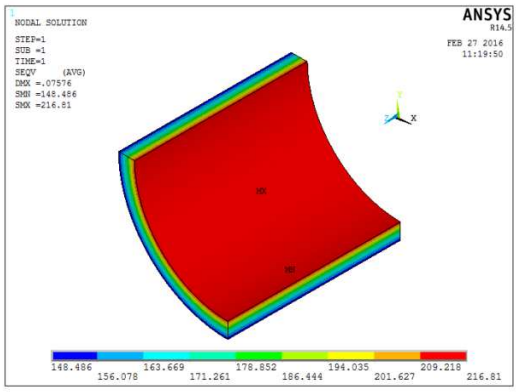

Fig. 13. Von Mises stress - Elastic model without nozzle

Figure 14 and 15 shows the hoop and Von mises stresses along the defined path (path A in Figure 5). From the same model solution, results for other parameters such as longitudinal stress, radial stress and stress intensity that occurs in the pressure vessel wall may be assessed in a similar manner if required.

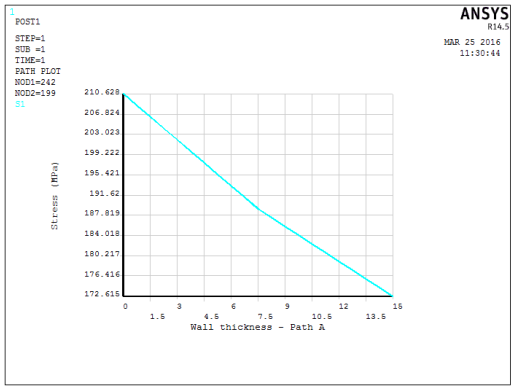

Fig. 14. Hoop stress along path A - Elastic model without nozzle

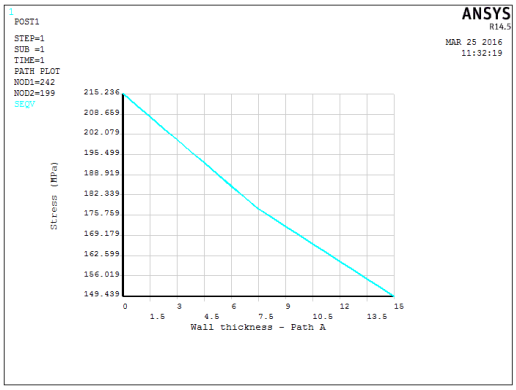

Fig. 15. Von Mises stress along path A - Elastic model without nozzle

Sometimes, it may be necessary to know the exact values of induced stress at various specific points on a component. This can be enabled by using the "Query Results" command through selecting the desired component and then picking the appropriate node on the specified point or region. It may be helpful to zoom in on the particular region. Figure 16 shows the values of hoop stress at various chosen points on the wall of the pressure vessel.

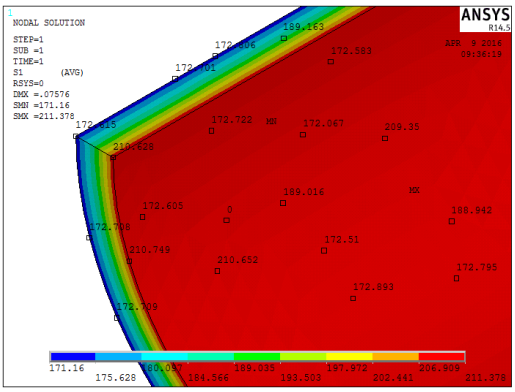

Fig. 16. Values of Hoop stress at various points

Figure 17 shows the deformed shape, while Figure 18 illustrates the resultant (vector sum) displacement that occurs. From the same model solution obtained, lateral (X-axis) and axial (Z-axis) direction displacement results can likewise be examined.

B. Elastic Analysis Results - Thick-walled Pressure Vessel With a Nozzle

Figure 19 and 20 illustrates FEA results for hoop and Von mises stress that occurs in the wall of the pressure vessel respectively.

Figure 21 and 22 respectively illustrates the hoop and Von mises stresses along path B. Figure 23 shows the resultant displacement that occurs.

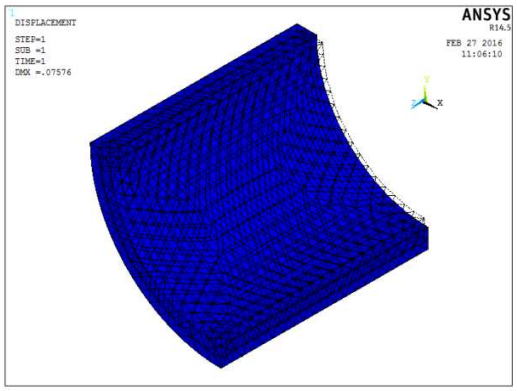

Fig. 17. Deformed shape - Elastic model without nozzle

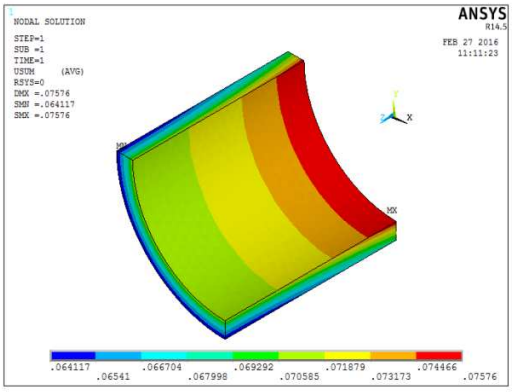

Fig. 18. Resultant displacement - Elastic model without nozzle

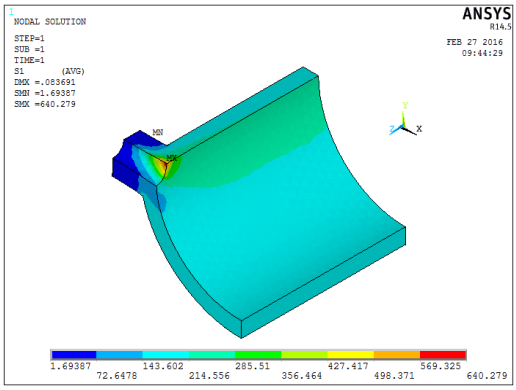

Fig. 19. Hoop stress - Elastic model with nozzle

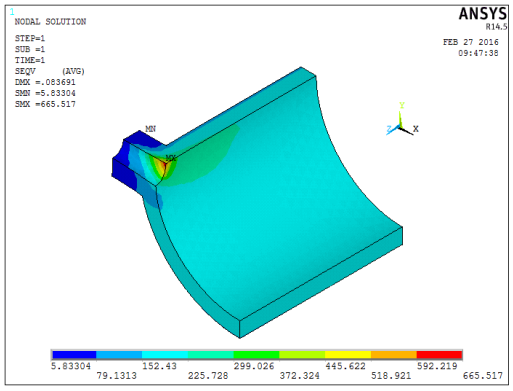

Fig. 20. Von Mises stress - Elastic model with nozzle

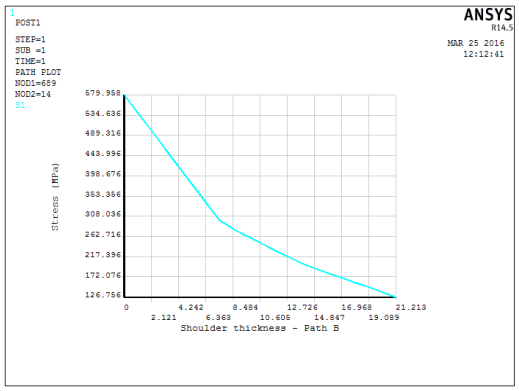

Fig. 21. Hoop stress on path B - Elastic model with nozzle

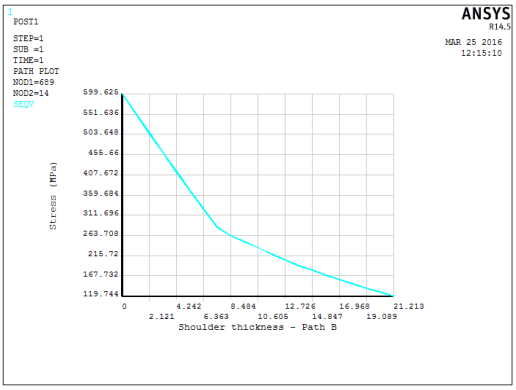

Fig. 22. Von Mises stress on path B - Elastic model with nozzle

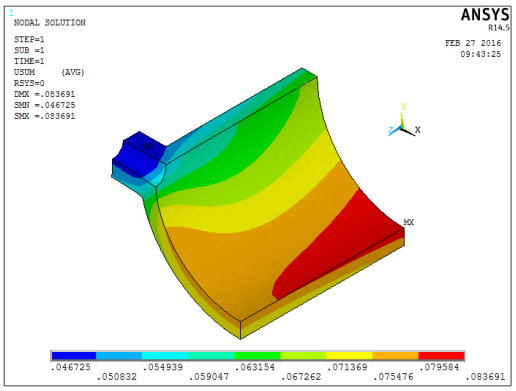

Fig. 23. Resultant displacement - Elastic model with nozzle

C. Plastic Analysis Results - Thick-walled Pressure Vessel Without a Nozzle

1) FE Plastic Analysis - Plastic Region of $5mm$ *Depth:* From the FEA solution, Figure 24 and 25 respectively shows the hoop and Von Mises stress that occurs on the pressure vessel wall. Figure 26 and 27 , respectively illustrates the hoop and Von Mises stress distribution across the wall thickness along path A (see Figure 5). Figure 28 shows the resultant displacement that occurs.

2) FE Plastic Analysis - Plastic Region of $10mm$ *Depth:* From the FEA solution, Figure 29 and 30 respectively shows the hoop and Von Mises stress that occurs on the vessel wall.

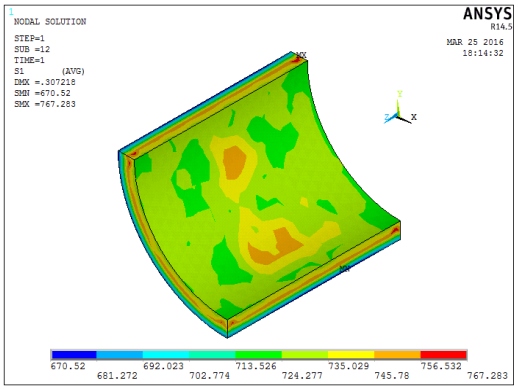

Fig. 24. Hoop stress - Plastic model without nozzle: $r_c = 80mm$

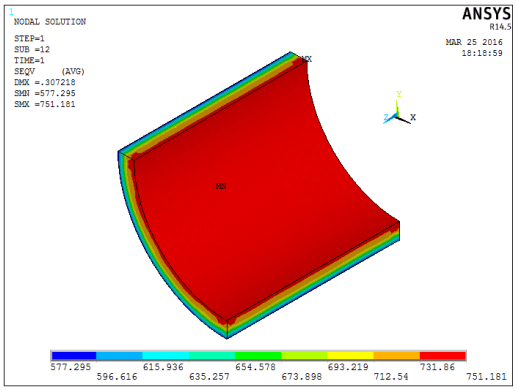

Fig. 25. Von Mises stress - Plastic model without nozzle: $r_c = 80mm$

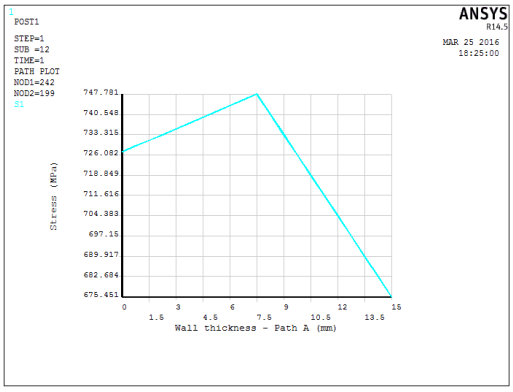

Fig. 26. Hoop stress on path A - Plastic model without nozzle: $r_c = 80mm$

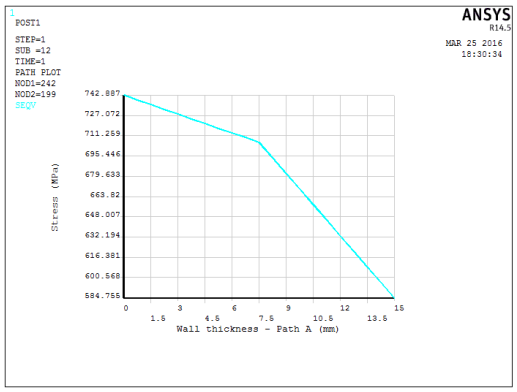

Fig. 27. Von Mises stress on path A - Plastic model without nozzle: $r_c = 80mm$

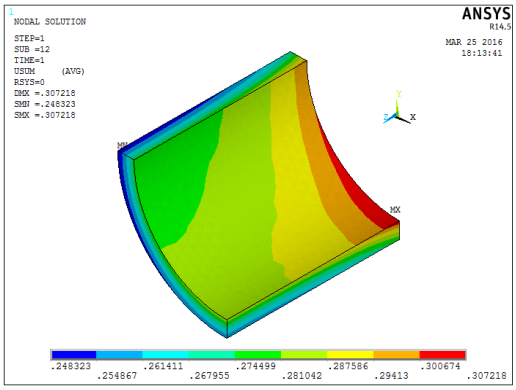

Fig. 28. Resultant displacement - Plastic model without nozzle: $r_c = 80mm$

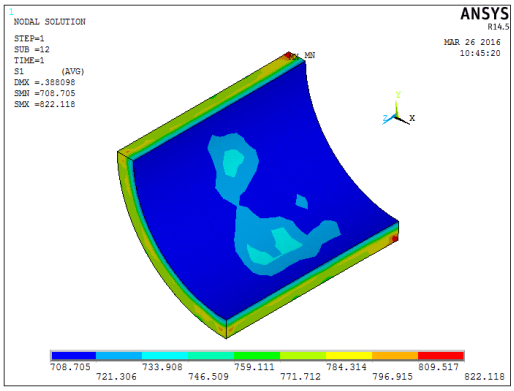

Fig. 29. Hoop stress - Plastic model without nozzle: $r_c = 85mm$

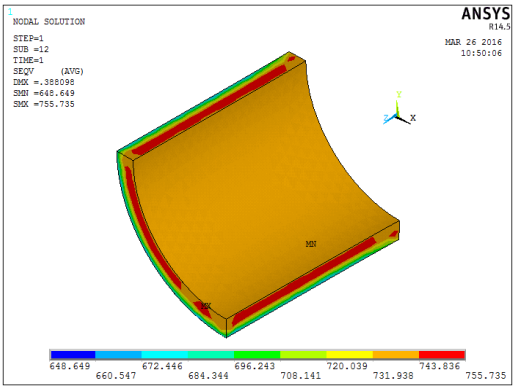

Fig. 30. Von Mises stress - Plastic model without nozzle: $r_c = 85mm$

Figure 31 and 32, respectively illustrates the hoop and Von Mises stress distribution across the wall thickness along path A. Figure 33 shows the resultant displacement that occurs.

D. Plastic Analysis Results - Thick-walled Pressure Vessel With a Nozzle

From the results obtained, Figure 34 and 35 respectively shows the hoop and Von Mises stress induced in the wall of the pressure vessel.

Figure 36 and 37 respectively illustrates the hoop and Von Mises stress distribution along path B (see Figure 8) around the nozzle neck within the pressure vessel wall. Figure 38 shows the resultant displacement that occurs.

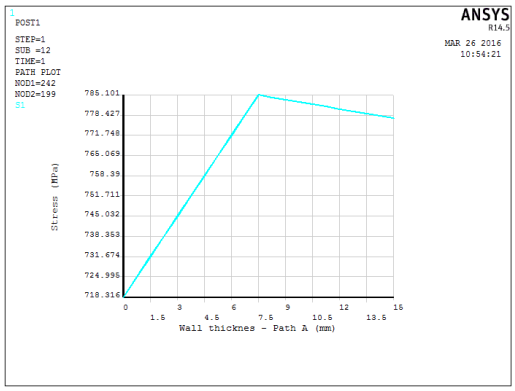

Fig. 31. Hoop stress on path A - Plastic model without nozzle: $r_c = 85mm$

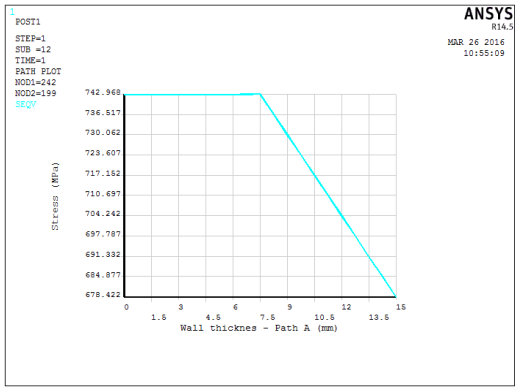

Fig. 32. Von Mises stress on path A - Plastic model without nozzle: $r_c = 85mm$

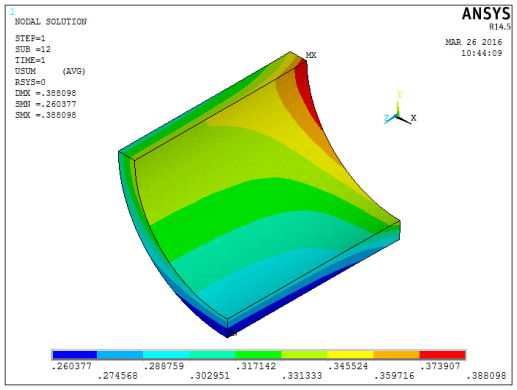

Fig. 33. Resultant displacement - Plastic model without nozzle: $r_c = 85mm$

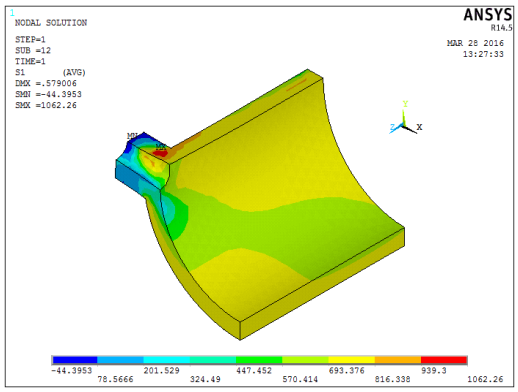

Fig. 34. Hoop stress - Plastic model with nozzle: $r_c = 80mm$

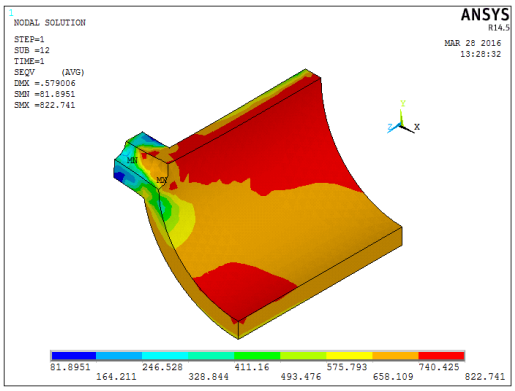

Fig. 35. Von Mises stress - Plastic model with nozzle: $r_c = 80mm$

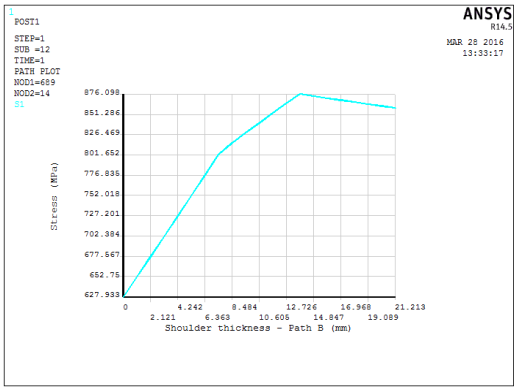

Fig. 36. Hoop stress on path B - Plastic model with nozzle: $r_c = 80mm$

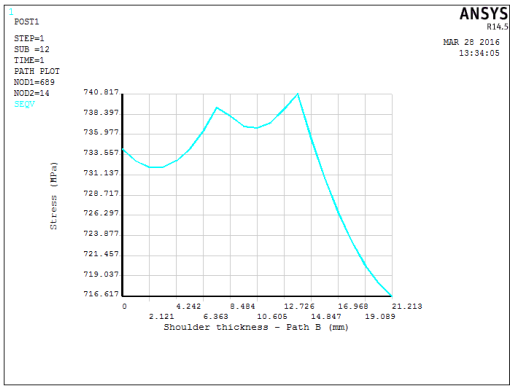

Fig. 37. Von Mises stress on path B - Plastic model with nozzle: $r_c = 80mm$

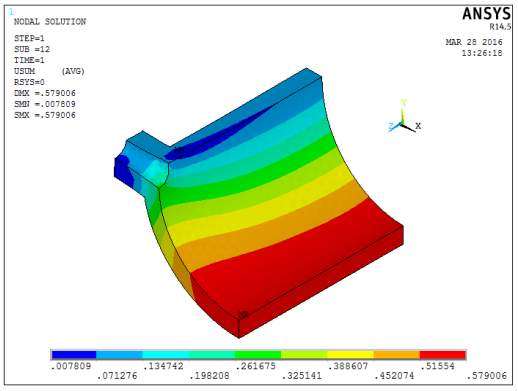

Fig. 38. Resultant displacement - Plastic model with nozzle: $r_c = 80mm$

E. Discussion of Results

Table II shows a summary of Elastic FEA results obtained from all the cases considered including some theoretical (calculated) results for comparison. A summary of Plastic analysis results from the study are listed in Table III. From the results in Table II, it is observed that there is a close agreement of the FEA results and the calculated results. This validates the FEA results and in this case provides the reliability and accuracy of the results obtained. From Table III, the FEA and the calculated results have slightly bigger margin. The reason for that was not certainly established, but could have probably been due to the material's behaviour model that was assumed in the study. The assumption was of elastic-perfectly plastic material, which does not exhibit strain hardening, that is, a material whose strain hardening exponent is zero. However, the value of the strain exponent is expected to be less than 0.2, like for most structural engineering materials and therefore the difference of the theoretical and FEA results could not have been that significant due to this assumption, which is generally recommended.

TABLE II
ELASTIC ANALYSIS RESULTS - MAXIMUM STRESSES AND DISPLACEMENT

Pressure Vessel Geometry	Pressure Vessel Geometrical Size (R_1/t)	Max. Hoop Stress (MPa)	Cal. Max. Hoop Stress (MP)	Max. Von Mises Stress (MPa)	Cal. Von Mises Stress (MPa)	Max. Displacement (mm)
Without Nozzle	3	139.098	135.7143	151.996	150.4410	0.032257
	5	212.38	210.7273	216.810	215.4040	0.07576
	8	325.435	324.1176	314.096	313.6030	0.175468
	10	400.756	399.9048	379.761	379.2367	0.26527
With Nozzle	3	428.773	-	440.014	-	0.35086
	5	640.279	-	665.517	-	0.86691
	8	955.753	-	966.287	-	0.196851
	10	1167.05	-	1172.07	-	0.296565

TABLE III
PLASTIC ANALYSIS RESULTS - MAXIMUM STRESSES AND DISPLACEMENT

Pressure Vessel Geometry	Pressure Vessel Geometrical Size (R_1/t)	Max. Hoop Stress (MPa)	Max. Von Mises Stress (MPa)	Max. Displacement (mm)	Hoop Stress at R_1 on path A (MPa)	Cal. Hoop Stress at R_1 on path A (MPa)
Without Nozzle: Plastic zone=5mm	3	723.268	757.82	0.205363	660.673	636.47
	5	767.283	751.151	0.307218	727.223	712.54
	8	795.957	747.595	0.457896	771.025	761.72
	10	806.585	745.938	0.564092	786.827	779.39
Without Nozzle: Plastic zone=10mm	3	812.527	762.154	0.279046	640.503	617.26
	5	822.118	755.735	0.388098	718.316	704.22
	8	831.763	751.621	0.520035	767.054	761.72
	10	836..280	750.921	0.634983	784.177	779.39
With Nozzle: Plastic zone =5mm	3	1224.25	986.631	0.417947	-	-
	5	1062.26	822.741	0.579006	-	-
	8	1055.42	806.242	1.00278	-	-
	10	1095.55	853.889	1.29771	-	-

The values of hoop and Von mises stress from Table II are observed to increase proportionally with the increase of R_1 to t ratio, for the same operating internal pressure of $38MPa$. The resulting hoop and Von mises stresses are found to register the largest values at the region around the nozzle in both the elastic and plastic analysis. This is a reasonable observation since stresses normally tend to concentrate at regions with geometric discontinuity like around the nozzle.

Stress distribution across the wall thickness (along path A) showed a linear variation of the stresses in all the cases considered. In the elastic analysis, the hoop and Von Mises stress variation registered a maximum value on the inner surface and a minimum value on the outer surface of the pressure vessel wall (see Figure 14 and 15). This was as theoretically expected and generally, the results closely agreed with the calculated results (see Table II). On the other hand, in the plastic analysis with an estimated plastic region depth of 5 mm, the hoop stress increased linearly from the inner surface to a maximum value at the point corresponding with the approximated plastic region depth (7.5 mm) and then decreased linearly to a minimum value at the outer surface (see Figure 26). Von mises stress decreased linearly from a maximum value (approximated to yield point stress, 743 MPa) up to a certain point and then the decrease continued with slightly higher slope up to the outside surface along path A. When the estimated depth of plastic region was increased to 10 mm, the value of hoop stress increased linearly from a minimum value up to the maximum value at the plastic-elastic transition point and then the stress decreased linearly and slightly up to the outer surface (see Figure 31)). Von Mises stress remained constant at a maximum value approximated to the yield point stress (743 MPa) from the inner surface up to the approximated plastic region depth of 7.5 (see Figure 32). This kind of representation was similar for all the cases considered, with a resulting plastic region depth maintained to 7.5 mm. The plastic analysis results showed a less accurate theoretical prediction (see Table III) for reasons attributed to what has been explained earlier.

Stress distribution within the pressure vessel wall around the nozzle neck (along path B) and across the wall thickness along path A showed completely different results. In the elastic analyses, both the hoop and the Von Mises stress distribution varied in a similar manner. The value of stress decreased linearly from a maximum value on the inner surface to a certain point and then the decrease continued with a slightly lower slope up to the minimum value on the outer surface along path B (see Figure 21). In the plastic analyses, the variation of hoop stress increased linearly from the minimum value on the inner surface and then the increase continued but with slightly lower slope up to the maximum value from where a linear decrease of the stress slightly occurred up to the outer surface along Path B (see Figure 36). Von Mises stress distribution along path B showed a peculiar variation which assumed somehow a serial-parabolic shape (see Figure 37). Generally, the resulting representation of stress distribution around the nozzle neck was difficult to predict theoretically.

Von Mises failure criterion was applied in deriving the FEA stress-strain material behaviour model (Figure 11) that was used in the plastic analysis. As a result, fully plastic state was attained when the Von Mises stress approximated to the material's yield strength of $743MPa$ (see Figure 32).

The amount of deformation that occurred was relatively higher in the plastic analyses compared to that in the elastic analyses. This was as expected and generally, the maximum values recorded for all the cases considered were hardly greater than 1 millimetre, except for only two cases which showed slightly greater values (see tables II and III).

Therefore, it can be deduced that the maximum expansion (deformation) of the pressure vessel that would occur is very small and physically unnoticeable.

When the depth of the plastic region was increased to $10mm$ for plastic analysis using the model with a nozzle geometry included, the solution failed to give any results. The interpretation to the outcome report that, the component was improperly constrained, was the assumption that some parts (seen as not properly constrained) of the pressure vessel had started to fail due to increased loading. The critical areas probably to have started failing were those around the nozzle.

V. CONCLUSIONS

1) Stress distribution in the elastic stress state was found to be totally different to that in the plastic stress state of a thick-walled pressure vessel. In the elastic stress state, both the hoop and the Von Mises stress distribution varies exactly in a similar manner, even on the areas with geometric discontinuity, like around the nozzle neck (compare Figure 14 and 15 and also compare Figure 21 and 22). In the plastic stress state, the hoop and Von Mises stress distribution varies differently only in the plastic region (compare Figure 31 and 32). In the areas with stress concentration around the nozzle neck, hoop and Von Mises stress distribution are totally different (Compare Figure 36 and 37).

2) Stress distribution in a pressure vessel is affected significantly by having geometric discontinuities like the nozzle. The presence of the nozzle,which causes stress concentration around the neck region as expected, affects the stress distribution, not only locally, but in a large portion of the pressure vessel.

3) For the same internal pressure, both hoop and Von Mises stress increases proportionally with the increase of R_1 to t ratio of a pressure vessel.

4) It is was not possible to increase the plastic region to a depth of 10 mm for the geometrical model with a nozzle geometry included. In cases where geometric discontinuities like the nozzle exists, abrupt rise in stress levels (stress concentrations) occurs in areas such as around the nozzle neck, which subsequently leads to early failure before the whole section becomes fully plastic. As a result, this may inhibit making of a fully autofrettaged pressure vessel, which requires loading of the pressure vessel to fully plastic state.

REFERENCES

[1] Raju G., Hari K. Babu, Siva Nagaraju N. and Kirau K., "Design and analysis of stress on thick-walled cylinder with and without holes", International Journal of Engineering Research and Applications, vol. 5, 2015, pp. 75-83.
[2] Dr. Clemens Kaminski, "Stress analysis of prewssure vessels" University of Cambridge, 2005.
[3] Prem N., "Pressure vessel design", Tech rep., Safetyline Institute Work and Safety Practitioner, Department of Commerce State of Western Australia, 2012.
[4] Denne M., "Pressure vessel design manual, third edition" Gulf Professional publishing, 2004.
[5] Liu P.F. and Zheng J.Y., "Finite element analysis of tensile behaviour of ductile steel with defects ", Technical artical - Peer Reviewed: Journal of failure analysis and prevention, vol.10, 2010, pp. 212-217.
[6] Thomas Davidson E. and David Kendall P., "The design of pressure vessels for very high pressure operation", Tech rep., Benet R & E Laboratories - Watervliet Arsenal, Newyork, 1969.
[7] Digvjay Kolekar and Jewargi S.S., "Stress analysis of pressure vessel with different type of end connections - A review", International Journal of Science, Engineering and Technology Research (IJSETR), vol. 3, 2014.
[8] Mutahir Ahmed, Rafi Ullah Khan, Saeed Badshah and Sakhi Jan, "Finite element investigation of geometry effect on pressure vessel under combined structural and thermal loads", International Journal of Engineering and Advanced Technology (IJEAT), vol4, 2014.
[9] Somnath C., "Pressure vessels design and practice - Overview of pressure vessels", Tech rep., Mechanical and Aerospace Engineering series, 2005.
[10] Amrab Ayob, M. Kabashi Elbasheer, "Optimum autofrettage pressure in thick cylinders", Journal Mekanikal, vol. 24, 2014, pp. 1-14.
[11] D. Dinesh Babu and Tegan Balaji T., "Theoretical and finite element analysis of high pressure components", IOSR Journal of Engineering (IOSRJEN), vol.3, 2013, pp. 25-34.